






Article

Mono-, Di-, Tri-Pyrene Substituted Cyclic Triimidazole: A Family of Highly Emissive and RTP Chromophores

Daniele Malpicci ^{1,2} , Clelia Giannini ¹ , Elena Lucenti ^{2,3} , Alessandra Forni ^{2,3,*} , Daniele Marinotto ^{2,3} and Elena Cariati ^{1,2,3,*} 

¹ Department of Chemistry, Università degli Studi di Milano, Via Golgi 19, 20133 Milano, Italy; daniele.malpicci@unimi.it (D.M.); clelia.giannini@unimi.it (C.G.)

² Institute of Chemical Sciences and Technologies “Giulio Natta” (CNR-SCITEC), Via Golgi 19, 20133 Milano, Italy; elena.lucenti@scitec.cnr.it (E.L.); daniele.marinotto@scitec.cnr.it (D.M.)

³ INSTM RU, Via Golgi 19, 20133 Milano, Italy

* Correspondence: alessandra.forni@scitec.cnr.it (A.F.); elena.cariati@unimi.it (E.C.)

Abstract: The search of new organic emitters is receiving a strong motivation by the development of ORTP materials. In the present study we report on the preparation, optical and photophysical characterization, by both steady state and time resolved techniques, of two pyrene-functionalized cyclic triimidazole derivatives. Together with the already reported mono-substituted derivative, the di- and tri-substituted members of the family have revealed as intriguing emitters characterized by impressive quantum yields in solution and RTP properties in the solid state. In particular, phosphorescence lifetimes increase from 5.19 to 20.54 and 40.62 ms for mono-, di- and trisubstituted compounds, respectively. Based on spectroscopical results and theoretical DFT/TDDFT calculations on the di-pyrene molecule, differences in photophysical performances of the three compounds have been assigned to intermolecular interactions increasing with the number of pyrene moieties appended to the cyclic triimidazole scaffold.

Keywords: fluorescence; organic room temperature phosphorescence; DFT and TDDFT calculations



Citation: Malpicci, D.; Giannini, C.; Lucenti, E.; Forni, A.; Marinotto, D.; Cariati, E. Mono-, Di-, Tri-Pyrene Substituted Cyclic Triimidazole: A Family of Highly Emissive and RTP Chromophores. *Photochem* **2021**, *1*, 477–487. <https://doi.org/10.3390/photochem1030031>

Academic Editor: Marcelo I. Guzman

Received: 15 October 2021

Accepted: 16 November 2021

Published: 18 November 2021

Publisher's Note: MDPI stays neutral with regard to jurisdictional claims in published maps and institutional affiliations.



Copyright: © 2021 by the authors. Licensee MDPI, Basel, Switzerland. This article is an open access article distributed under the terms and conditions of the Creative Commons Attribution (CC BY) license (<https://creativecommons.org/licenses/by/4.0/>).

1. Introduction

Organic room temperature phosphorescent materials (ORTP), due to their increased biocompatibility and reduced cost with respect to their organometallic counterparts, are the subject of intense research in the field of functional materials, appearing promising for applications spanning from bioimaging [1,2] to anti-counterfeiting [3,4] and displays [5]. Many strategies have been developed to realize ORTP materials. Among them, $\pi \cdots \pi$ stacking interactions [6–8], host–guest systems [9–11], co-assembly based on macrocyclic compounds [12], crystallization [13–15], halogen bonding [16,17], and doping in a polymer matrix [18], can be mentioned. Triimidazo[1,2-*a*:1',2'-*c*:1'',2''-*e*][1,3,5]triazine, **TT** [7], is the prototype of a family of ORTP materials, showing in the crystalline phase ultralong phosphorescence (up to 1 s) associated with the presence of strong $\pi \cdots \pi$ stacking interactions [6]. Introduction of one or multiple halogen atoms on the **TT** scaffold results in a complex excitation dependent photoluminescent behavior including dual fluorescence, molecular and supramolecular phosphorescences, together with ultralong components [8,19–21]. The introduction of one chromophoric fragment, namely 2-fluoropyridine, 2-pyridine and pyrene (**TTPyr₁**) has further enriched the photophysical behavior, preserving the solid state ultralong component [22–24]. In particular, the pyrene functionality was chosen due to its favorable emissive properties (i.e., high fluorescence quantum efficiency and good hole-transporting ability) which can be exploited in a large number of applications [25–27]. **TTPyr₁** was isolated and characterized in two solvated phases and two not solvated polymorphs. In particular, the two solvated and one polymorph, belonging to centrosymmetric space groups, are obtained at room temperature, while a non-centrosymmetric polymorph

can be irreversibly prepared by proper thermal treatment in air starting from the room temperature phases. While in solution the chromophore is characterized by a single fluorescence (quantum yield $\Phi = 90\%$, see Table 1), in the solid state intermolecular interactions impart rigidification to the molecule favoring the appearance of a long-lived component whose lifetime and intensity strongly depend on the crystallinity of the sample. Moreover, differently from the room temperature phases, the non-centrosymmetric one displays not only second order nonlinear optical features (SHG ten times that of standard urea), but also an additional fluorescence associated with the presence of two possible almost isoenergetic conformers in its crystals. Additionally, the material in aggregate-state was tested for cellular and bacterial imaging in view of its applications in bioimaging [24].

Table 1. Photophysical parameters of Pyrene, TTPyr₁, TTPyr₂ and TTPyr₃ at 298 K.

		Φ %	λ_{em} (nm)	τ_{av}	k_r (10^7 s ⁻¹)	k_{nr} (10^7 s ⁻¹)
Pyrene	DMSO (2.5×10^{-6} M)	33.4	374	94.15 ns	0.355	0.707
	DMSO (10^{-5} M)	92	420	2.76 ns	33.3	2.90
TTPyr ₁	Ground Crystal (TTPyr RT)	54	475 514	2.15 ns 5.19 ms	25.1	21.4
	DMSO (2.5×10^{-6} M)	78	419	9.22 ns	8.46	2.39
TTPyr ₂	Powders	40.2	490 528	4.64 ns 20.54 ms	8.66	12.9
	DMSO (2.5×10^{-6} M)	74.4	422	11.16 ns	6.67	2.29
TTPyr ₃	Powders	36.9	476 522	5.12 ns 40.62 ms	7.21	12.3

Here, we report the synthesis, characterization and photophysical studies of the analogue derivatives with two and three pyrene moieties on the TT scaffold, TTPyr₂ and TTPyr₃, respectively. The photophysical behavior of the solid compounds, comprising one fluorescence and one phosphorescence, is similar to that of TTPyr₁ in the room temperature phases. However, a systematic increase of the phosphorescence lifetime is observed by increasing the number of pyrene groups. Unfortunately, due to the impossibility to get single crystals suitable for X-ray diffraction analysis, an explanation of this phenomenon can be given only at a qualitative level.

2. Materials and Methods

All reagents were purchased from chemical suppliers and used without further purification. Pyrene was crystallized from hot toluene solution before photoluminescence measurements. Triimidazo[1,2-*a*:1',2'-*c*:1'',2''-*e*][1,3,5]triazine (TT) [28], its dibromo- and tribromo-derivatives (namely 3,7-dibromotriimidazo[1,2-*a*:1',2'-*c*:1'',2''-*e*][1,3,5]triazine, TTBr₂, and 3,7,11-tribromotriimidazo[1,2-*a*:1',2'-*c*:1'',2''-*e*][1,3,5]triazine, TTBr₃) [19] and TTPyr₁ [24] were prepared according to literature procedures.

¹H and ¹³C NMR spectra were recorded on a Bruker AVANCE-400 instrument (400 MHz). Chemical shifts are reported in parts per million (ppm) and are referenced to the residual solvent peak (DMSO, ¹H 2.50 ppm, ¹³C 39.5 ppm; CH₂Cl₂, ¹H 5.32 ppm, ¹³C 54.0 ppm). Coupling constants (*J*) are given in hertz (Hz) and are quoted to the nearest 0.5 Hz. Peak multiplicities are described in the following way: s, singlet; d, doublet; m, multiplet.

Mass spectra were recorded on a Thermo Fisher (Thermo Fisher Scientific, Waltham, MA USA) LCQ Fleet Ion Trap Mass Spectrometer equipped with UltiMate™ 3000 HPLC system. UV-Visible spectra were collected by a Shimadzu UV3600 spectrophotometer (Shimadzu Italia S.r.l., Milan, Italy).

Absolute photoluminescence quantum yields were measured using a C11347 (Hamamatsu Photonics K.K). A description of the experimental setup and measurement method can be found in the article of K. Suzuki et al. [29]. For any fixed excitation wavelength, the fluorescence quantum yield Φ is given by:

$$\Phi = \frac{\text{PN(Em)}}{\text{PN(Abs)}} = \frac{\int \frac{\lambda}{hc} \left[I_{\text{em}}^{\text{sample}}(\lambda) - I_{\text{em}}^{\text{reference}}(\lambda) \right] d\lambda}{\int \frac{\lambda}{hc} \left[I_{\text{ex}}^{\text{reference}}(\lambda) - I_{\text{ex}}^{\text{sample}}(\lambda) \right] d\lambda}$$

where PN(Em) is the number of photons emitted from a sample and PN(Abs) is the number of photons absorbed by a sample, λ is the wavelength, h is Planck's constant, c is the velocity of light, $I_{\text{em}}^{\text{sample}}(\lambda)$ and $I_{\text{em}}^{\text{reference}}(\lambda)$ are the photoluminescence intensities with and without a sample, respectively, $I_{\text{ex}}^{\text{sample}}(\lambda)$ and $I_{\text{ex}}^{\text{reference}}(\lambda)$ are the integrated intensities of the excitation light with and without a sample, respectively. PN(Em) is calculated in the wavelength interval $[\lambda_i, \lambda_f]$, where λ_i is taken 10 nm below the excitation wavelength, while λ_f is the upper end wavelength in the emission spectrum. The error made was estimated at around 5%.

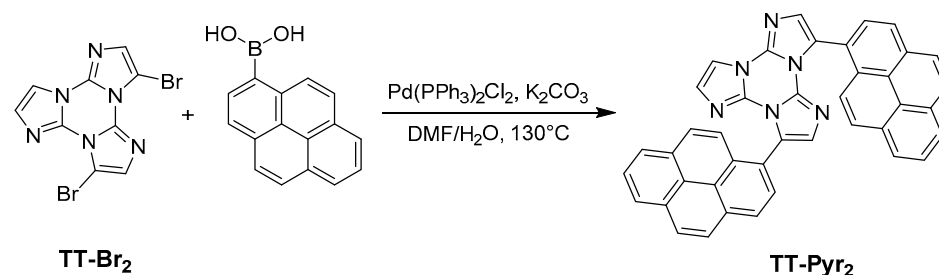
Steady state emission and excitation spectra and photoluminescence lifetimes were obtained using a FLS 980 (Edinburgh Instrument Ltd., Livingston, United Kingdom) spectrofluorimeter. The steady state measurements were recorded by a 450 W Xenon arc lamp. Photoluminescence lifetime measurements were performed using: Edinburgh Picosecond Pulsed Diode Laser EPL-375, EPLED-300, (Edinburgh Instrument Ltd.) and microsecond flash Xe-lamp (60 W, 0.1 ÷ 100 Hz) with data acquisition devices time correlated single-photon counting (TCSPC) and multi-channel scaling (MCS) methods, respectively. Average lifetimes are obtained as:

$$\tau_{\text{av}} \equiv \frac{\sum_{n=1}^m \alpha_n \tau_n^2}{\sum_{n=1}^m \alpha_n \tau_n},$$

where m is the multi-exponential decay number of the fit.

2.1. Synthesis of 3,7-Di(pyren-1-yl)triimidazo[1,2-a:1',2'-c:1'',2''-e][1,3,5]triazine (TT-Pyr₂)

TT-Pyr₂ was prepared by Suzuki coupling between TT-Br₂ and pyrene-1-boronic acid (see Scheme 1). In a typical reaction, TT-Br₂ (595 mg; 1.67 mmol), pyrene-1-ylboronic acid (970 mg, 3.94 mmol), Pd(PPh₃)₂Cl₂ (170 mg, 0.24 mmol), water (3 mL) and DMF (25 mL) were transferred inside a 100 mL Schlenk flask equipped with a magnetic stirrer. The system was heated under static nitrogen atmosphere at 130 °C for 12 h. The reaction was then cooled to room temperature, precipitated with water (200 mL) and filtered on a Büchner. The solid crude reaction mixture was further purified by automated flash chromatography on SiO₂ with DCM/CH₃CN as eluents to give the TT-Pyr₂ product as a yellow solid (724 mg; Yield 72%; R_f = 0.5 in DCM/CH₃CN = 95/5).



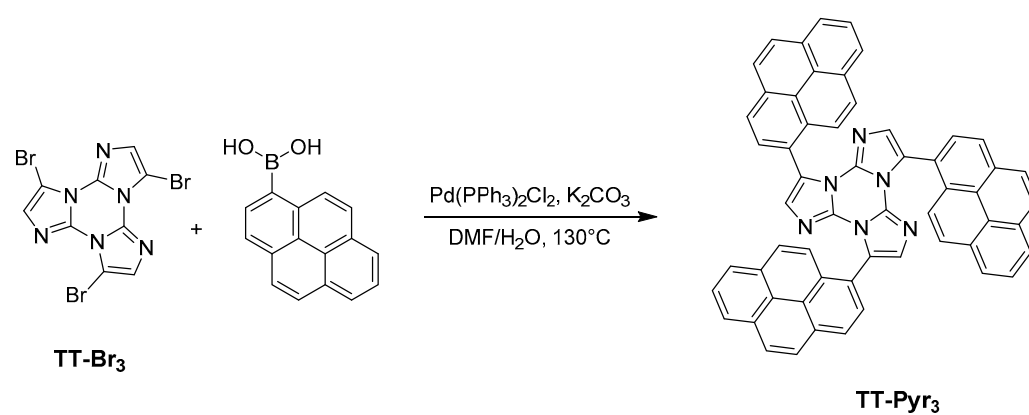
Scheme 1. Synthetic path for the preparation of TT-Pyr₂.

NMR data (9.4 T, DMSO-d₆, 298 K, δ , ppm): ¹H NMR 8.46–8.07 (18H, m), 8.01 (1H, d, $J = 1.5$ Hz), 7.53 (1H, s), 6.98 (1H, s), 6.88 (1H, d, $J = 1.5$ Hz); ¹³C NMR 136.7, 136.6, 135.9, 131.4, 131.3, 130.9, 130.7, 130.4, 130.3, 129.8, 129.5, 128.8, 128.4, 128.2, 128.1, 128.0, 127.7, 127.5, 127.3, 127.2, 126.4, 125.7, 125.6, 125.4, 124.3, 124.2, 124.1, 123.7, 123.6, 123.5, 110.9.

MS (ESI-positive ion mode): m/z : 599 [M + H]⁺.

2.2. Synthesis of 3,7,11-Tri(pyren-1-yl)triimidazo[1,2-a:1',2'-c:1'',2''-e][1,3,5]triazine (TT-Pyr₃)

TT-Pyr₃ was prepared by Suzuki coupling between TT-Br₃ and pyrene-1-boronic acid (see Scheme 2). In a typical reaction, TT-Br₃ (400 mg; 0.91 mmol), pyrene-1-ylboronic acid (702 mg, 2.85 mmol), potassium carbonate (1.3 g, 9.19 mmol), Pd(PPh₃)₂Cl₂ (64 mg, 0.09 mmol), water (2 mL) and DMF (10 mL) were transferred inside a 100 mL Schlenk flask equipped with a magnetic stirrer. The system was heated under static nitrogen atmosphere at 130 °C for 12 h. The reaction was then cooled to room temperature, precipitated with water (200 mL) and filtered on a Büchner. The solid crude reaction mixture was further purified by automated flash chromatography on SiO₂ with Hexane/Et₂O/DCM as eluents to give the TT-Pyr₃ product as a pale yellow solid (435 mg; Yield 60%; R_f = 0.5 in Hexane/Et₂O/DCM = 60/20/20).



Scheme 2. Synthetic path for the preparation of TT-Pyr₃.

NMR data (9.4 T, CD₂Cl₂, 300 K, δ , ppm): ¹H NMR 8.34–8.06 (27H, m), 7.04 (3H, s); ¹³C NMR 136.9, 132.7, 131.9, 131.4, 130.3, 129.0, 128.8, 127.9, 126.9, 126.3, 126.1, 125.6, 125.1, 124.7, 123.7.

MS (ESI-positive ion mode): m/z : 799 [M + H]⁺.

2.3. Computational Details

Geometry optimization of TT-Pyr₂ has been performed at the ω B97X/6-311++G(d,p) level of theory [30], in agreement with the computational protocol previously developed to study TT [7] and its derivatives, in particular TT-Pyr₁ [24]. The adopted functional was in fact demonstrated to be able to accurately describe ground and excited states properties of TT and its derivatives, besides dispersive intermolecular interactions which are essential to interpret the multi-faceted properties of this family of compounds. Calculations on the tri-pyrene derivative have not been performed due to the required high computational costs. All calculations have been performed with Gaussian 16 [31].

3. Results

3.1. Synthesis and Molecular Structures

TT-Pyr₂ and TT-Pyr₃ were prepared by Suzuki coupling between pyrene-1-boronic acid and the corresponding di- and tri-brominated TT precursors (see Schemes 1 and 2). The new pyrene derivatives were characterized by ¹H and ¹³C NMR spectroscopy (Figures S1–S5) and mass spectrometry (Figures S3 and S6), samples with the purity grade required for photophysical characterization were obtained by repeated crystallizations.

In order to get insight on the structural features of the investigated compounds, DFT calculations were performed on the smaller derivative, TT-Pyr₂ (see optimized structures in Figure 1). Owing to the lack of the crystal structure of this compound, suitable models were built up starting from structural information previously obtained on TT-Pyr₁ by both X-ray

diffraction analysis and theoretical calculations [24]. For this latter compound, crystallizing in different phases and polymorphs, two possible conformations were detected, which correspond to different orientation of pyrene with respect to the **TT** moiety as denoted by the (H)C1-C2-C10-C11(H) torsion angle τ (C2-C10 being the bond connecting **TT** with pyrene). In particular, the room temperature phases display τ values equal to about 129° (RT conformation), while the polymorph obtained at high temperature shows τ equal to 49° (HT conformation) [24]. DFT geometry optimization of the two conformations leads to different almost isoenergetic minima (having $\tau = 110.3$ and 67.4° , respectively) in a very flat region. The HT conformation is only 0.6 kcal/mol more stable than the RT one, suggesting that both conformations are expected to be present in solution. To build up the **TTPyr₂** model, an additional pyrene moiety was added, in the proper position, to both the RT and HT optimized geometries of **TTPyr₁** imposing the same RT or HT conformation. The resulting optimized structures (see Figure 1), denoted respectively as ‘RT/RT’ and ‘HT/HT’ conformations, display C1–C2–C10–C11 and C1’–C2’–C10’–C11’ torsion angles equal to 112.3 and -67.2° (RT/RT) and 67.4 and 67.3° (HT/HT conformation), the latter being more stable by 0.54 kcal/mol. Of course, also the mixed ‘RT/HT’ conformation is envisaged to be present in solution, but no significant differences in the electronic levels are expected with respect to those computed by TDDFT for the RT/RT and HT/HT conformations, which are themselves very similar (see Table S1).

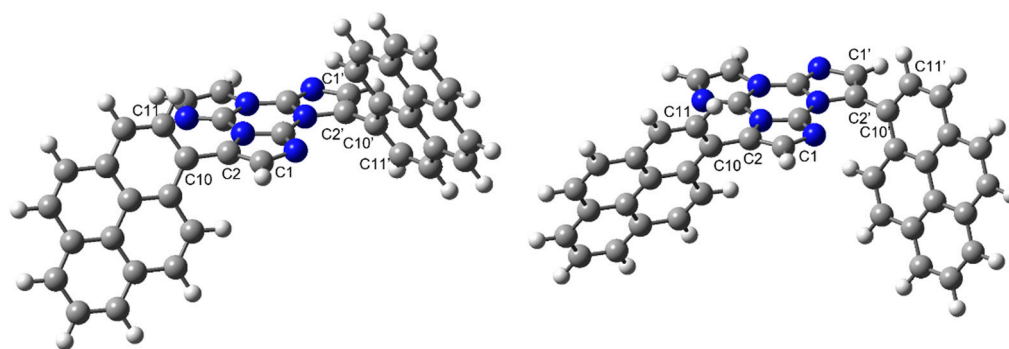


Figure 1. ω B97X/6-311++G(d,p) optimized geometry of **TTPyr₂** in the RT/RT (left) and HT/HT (right) conformations (hydrogen, carbon and nitrogen atoms in white, grey and blue, respectively).

Owing to the twisted arrangement of **TT** and pyrene in the investigated systems, a Quantum Theory of Atoms in Molecules (QTAIM) topological analysis [32] on the **TTPyr₁** and **TTPyr₂** electron density was performed to detect the possible presence of intramolecular interactions between the two moieties. In all cases, a bond critical point (bcp) between a **TT** nitrogen atom (N3) and the pyrene C10 carbon atom, located at about 3.18 \AA from each other, has been found ($\rho_{\text{bcp}} \sim 0.05 \text{ e \AA}^{-3}$, see Figures S7 and S8 for the **TTPyr₁** and **TTPyr₂** molecular graphs). Owing to the nature of the involved atoms, such $\text{N} \cdots \text{C}$ bond paths cannot be considered as classical non-covalent interactions [33], though contributing to stabilize the molecule due to the privileged electron-exchange channel associated with the bond path [34].

Interestingly, the molecular graphs substantially change when considering the optimized geometries of **TTPyr₁** and **TTPyr₂** in the excited state (see Figures S9 and S10). The relaxed S_1 geometries are characterized by lower molecular twisting than the ground state one. In particular, for **TTPyr₁** τ varies from 110.3 to 138.5° (RT conformation) and from 67.4 to 41.5° (HT conformation), respectively, with a concomitant shortening of the C2-C10 bond (from 1.478 to 1.435 \AA), implying a greater conjugation between the **TT** and pyrene moieties compared with the ground state [24]. For **TTPyr₂**, on the other hand, only one pyrene unit undergoes a substantial relaxation with respect to **TT**, τ varying from 112.3 to 139.0° (RT/RT conformation) and from 67.3 to 40.8° (HT/HT conformation). The corresponding C2–C10 bond shortens from 1.477 to 1.422 and 1.433 \AA (RT/RT and HT/HT conformation, respectively). For the other pyrene unit, τ shows only slight variations

(from -67.2 to -64.6° in the RT/RT conformation and from 67.4 to 64.0° in the HT/HT conformation) and the $C2'-C10'$ bond remains almost unvaried. These results indicate that, as determined for **TTPyr₁**, also **TTPyr₂** shows in the excited state a greater conjugation, which is however extended on **TT** and only one pyrene unit. The associated molecular graphs (see Figures S9 and S10) reveal, for both conformations of **TTPyr₁** and **TTPyr₂**, the formation of an intramolecular $C-H \cdots N$ hydrogen bond between the **TT** and pyrene moieties. This interaction stabilizes the two conformations in the excited state allowing to reduce the molecular twisting.

3.2. Photophysical Studies

TTPyr₂ and **TTPyr₃** have been photophysically characterized both in solution and in solid state by steady state and time resolved spectroscopy. The results are reported in Table 1 together with those previously obtained for the room temperature non-solvated species of **TTPyr₁** and those of pyrene molecule in the same conditions.

Diluted DMSO solutions of the three compounds show two absorptions with peaks at 257, 268, 279 nm (ES_2) and 332, 347 nm (ES_1) respectively, with molar absorption coefficients, ϵ , computed at 347 nm, equal to 34,894, 46,408 and 84,443 $M^{-1} cm^{-1}$ for **TTPyr₁**, **TTPyr₂** and **TTPyr₃**, respectively. Such bands, even though strongly red shifted and broadened with respect to the parent pyrene moiety (see Figure 2), are ascribed to transitions of main pyrene character, as previously suggested based on the similarity with the absorption spectrum of pyrene itself in the same conditions and theoretical calculations [24]. Looking at the HOMO and LUMO energies of pyrene, **TTPyr₁**, and **TTPyr₂**, it is found that, while the HOMO energy is almost constant along the series, the LUMO one significantly decreases (by 0.17 or 0.19 eV according to the conformation) from pyrene to **TTPyr₁**, and remains almost unvaried going to **TTPyr₂**.

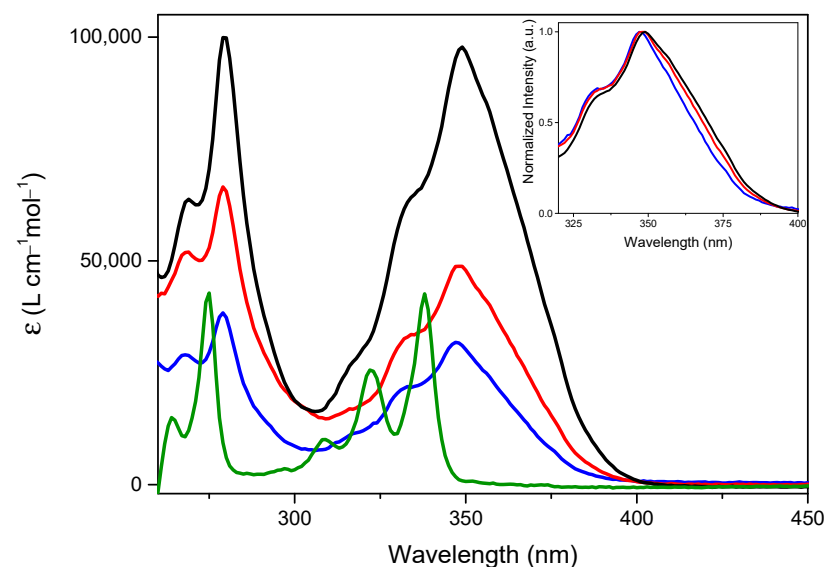


Figure 2. Molar absorption coefficient for $2.5 \cdot 10^{-6}$ M DMSO solution of **TTPyr₁** (blue line), **TTPyr₂** (red line), **TTPyr₃** (black line) and pyrene (green line). Inset: expansion of 350 nm region for normalized spectra of **TTPyr₁** (blue line), **TTPyr₂** (red line) and **TTPyr₃** (black line).

For the three compounds, perfectly overlapped emission spectra, consisting in an intense very broad single fluorescent emission at about 420 nm, are measured (see Figure 3). The three compounds display impressively high quantum yields when compared with pyrene itself ($\Phi = 33.4\%$) in the same conditions (see Table 1), suggesting that the **TT** moiety successfully suppresses the ACQ (aggregation caused quenching) phenomena affecting pyrene fluorescence [35–37]. Specifically, Φ equal to 92, 78 and 74% have been measured for **TTPyr₁**, **TTPyr₂**, **TTPyr₃**, respectively, with lifetime, τ , equal to 2.76 [24], 9.22 and 11.16 ns (Figures S11 and S14), resulting in k_f values 33.3, 8.46 and $6.67 \times 10^7 s^{-1}$ and k_{nr} 2.90, 2.39

and $2.29 \times 10^7 \text{ s}^{-1}$, respectively (see Table 1). The observed quantum yields are similar or higher than those reported in the literature for other mono-, di- and tri-pyrene substituted families. For example, DCM solutions of di- and tri-pyrene derivatives of carbazole and mono-, di- and tri-pyrene functionalized adamantane display Φ equal to 94 and 72% [32] and 17, 19 and 19% [38] respectively.

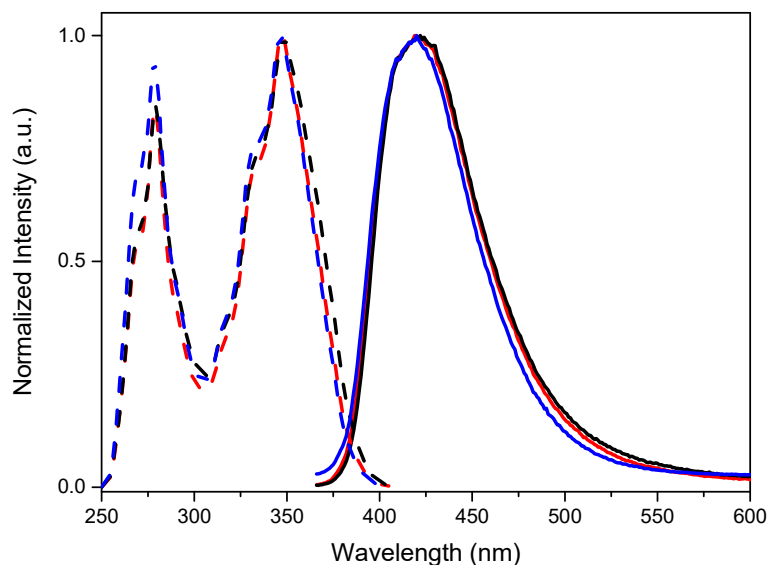


Figure 3. Normalized emission ($\lambda_{\text{exc}} = 350 \text{ nm}$, solid lines) and excitation ($\lambda_{\text{em}} = 420 \text{ nm}$, dashed lines) spectra of $2.5 \times 10^{-6} \text{ M}$ DMSO solutions at 298 K of **TTPyr₁** (blue line), **TTPyr₂** (red line) and **TTPyr₃** (black line).

To justify the slight decrease of quantum yield for **TTPyr₂** and **TTPyr₃** with respect to **TTPyr₁**, close inspection of optical properties has been performed. When better focusing on the 347 nm absorption of the three compounds (ES_1 , see inset of Figure 2), besides the already mentioned macroscopic red shift and broadening with respect to pyrene, a slight red shift and widening of the band from **TTPyr₁** to **TTPyr₂** and **TTPyr₃** can also be recognized. Based on DFT/TDDFT calculations, such band results from an envelope of more transitions (see Table S1 and Figures S20 and S21 for the simulated absorption spectra). In particular, two transitions are computed at low energy for pyrene (at 301 and 294 nm with oscillator strength $f = 0.0003$ and 0.347 , respectively) and **TTPyr₁** (at 304 and 302 nm with $f = 0.060$ and 0.498 , respectively), with a bathochromic displacement of the stronger transition and intensification of the low energy one, justifying the experimental red shift and broadening of **TTPyr₁** ES_1 . Going to **TTPyr₂**, four transitions are computed in the same region (at 306, 304, 303 and 301 nm with $f = 0.380, 0.101, 0.066$ and 0.445 , respectively, see Table S1 and Figures S20 and S21), implying further broadening of the associated band with very minor red shift with respect to **TTPyr₁**. It is as well to be taken into account that more conformations of similar energy are expected in solution, due to the flatness of the potential energy surface associated with the rotation of pyrene with respect to **TT** [24]. As reported in Table S1, such conformations are characterized by the same position of the transitions but slightly different oscillator strengths, further contributing to the band broadening. Similar results are expected for the tri-pyrene derivative, which was not submitted to theoretical calculations owing to the computational costs required by the further increased number of conformational degrees of freedom. Geometry optimization of S_1 for both conformations of **TTPyr₂** leads, as determined for **TTPyr₁**, to a reduced molecular twisting (see Figures S9 and S10) with a large energy separation from the higher excited states and approximately the same energy position ($\lambda = 372 \text{ nm}$), oscillator strength (0.693) and orbital composition (HOMO-LUMO with 93% weight) as found for **TTPyr₁** ($\lambda = 370 \text{ nm}$, $f = 0.698$, HOMO-LUMO with weight = 94%). Based on the strict similarity between **TTPyr₁** and **TTPyr₂** at molecular level, minor ACQ phenomena should be taken into account for **TTPyr₂**

and **TTPyr₃**. A similar result was previously obtained for pyrene-functionalized carbazole derivatives, with fluorescence quantum yield decreasing by increasing the number of pyrene moieties [39].

The three compounds are good emitters also in the solid state (see Table 1), where the emission is implemented by the presence, as already reported for **TTPyr₁** [24], of one phosphorescent component in addition to the fluorescent band (at 475, 490 and 476 nm for **TTPyr₁**, **TTPyr₂**, **TTPyr₃**, respectively, see Figure 4). The long lived component (at 514, 528 and 522 nm, with lifetimes equal to 5.19 [24], 20.54 and 40.62 ms for **TTPyr₁**, **TTPyr₂**, **TTPyr₃** respectively, see Figures S13 and S16) can be selectively activated by exciting at low energy (480 nm). Based on the conclusions drawn for **TTPyr₁** [24], even for **TTPyr₂** and **TTPyr₃** such long-lived emission could be explained by (i) easy singlet-to-triplet intersystem crossing due to almost overlapped singlet and triplet energy levels (see Figure S20), and (ii) interchromophoric interactions in the solid state which inhibit the molecular motions reducing the thermal non-radiative dissipation. Unfortunately, differently from **TTPyr₁** where such interactions have been deeply analyzed for the different isolated and crystallized phases, for **TTPyr₂** and **TTPyr₃** no single crystals suitable for X-ray diffraction analysis could be obtained. However, based on the longer lifetimes of **TTPyr₃**, a high number of interactions are expected for this latter with respect to the other members of the family. Such interactions are not efficacious for producing crystals due to the large number of conformational degrees of freedom (as expected, even though at lower extent, for **TTPyr₂**).

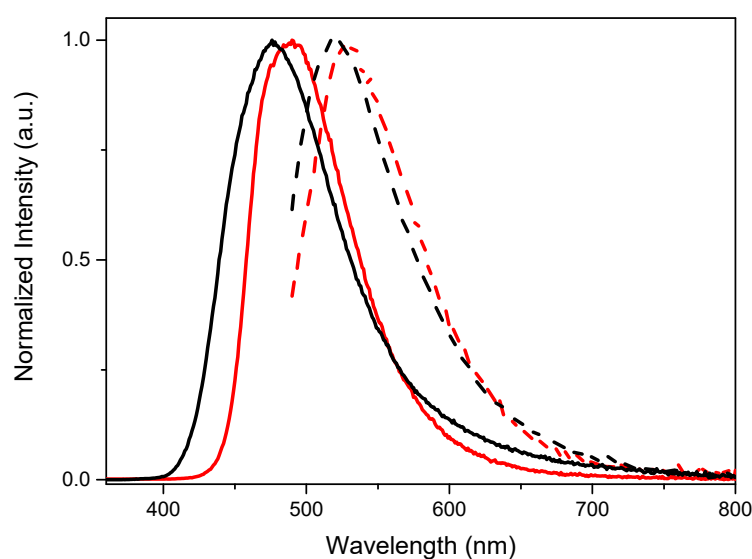


Figure 4. Normalized emission spectra ($\lambda_{\text{exc}} = 350$ nm solid line, $\lambda_{\text{exc}} = 480$ nm dashed line) at 298 K of powders of **TTPyr₂** (red) and **TTPyr₃** (black).

4. Conclusions

In conclusion, two new intriguing chromophores, **TTPyr₂** and **TTPyr₃**, have been prepared and characterized. Their photophysical behavior fully analyzed in solution and in solid state has been compared with that of parent **TTPyr₁** revealing a trend depending on the number of pyrene moieties appended to the **TT** scaffold. In particular, the fluorescence quantum yield in solution (much higher than that of pyrene itself) slightly decreases by increasing the number of pyrene units, while, in the solid state, the phosphorescent component, visible for all compounds at room temperature, possesses lifetimes increasing in the same order due to stabilizing interchromophoric interactions.

Supplementary Materials: The following are available online at <https://www.mdpi.com/article/10.3390/photochem1030031/s1>, **Figure S1.** ^1H NMR spectrum and expanded region of **TTPyr2** (400 MHz, DMSO- d_6), **Figure S2.** ^{13}C NMR spectrum and expanded region of **TTPyr2** (400 MHz, DMSO- d_6), **Figure S3.** LC-MS profile of **TTPyr2**, **Figure S4.** ^1H NMR spectrum and expanded region of **TTPyr3** (400 MHz, CD_2Cl_2), **Figure S5.** ^{13}C NMR spectrum and expanded region of **TTPyr3** (400 MHz, CD_2Cl_2), **Figure S6.** LC-MS profile of **TTPyr3**, **Figure S7.** Molecular graphs of **TTPyr1** in ground state RT (left) and HT (right) conformation with bond paths, bond critical points (green circles) and ring critical points (red circles), **Figure S8.** Molecular graphs of **TTPyr2** in ground state RT/RT (left) and HT/HT (right) conformation with bond paths, bond critical points (green circles) and ring critical points (red circles), **Figure S9.** Molecular graphs of **TTPyr1** in excited state RT (left) and HT (right) conformation with bond paths, bond critical points (green circles) and ring critical points (red circles), **Figure S10.** Molecular graphs of **TTPyr2** in excited state RT/RT (left) and HT/HT (right) conformation with bond paths, bond critical points (green circles) and ring critical points (red circles), **Figure S11.** Lifetime measurement (exc = 374 nm, em = 420 nm) of **TTPyr2** in DMSO at 298 K, **Figure S12.** Lifetime measurement (exc = 375 nm, em = 490 nm) of **TTPyr2** powders at 298 K, **Figure S13.** Lifetime measurement (exc = 340 nm, em = 530 nm) of **TTPyr2** powders at 298 K, **Figure S14.** Lifetime measurement (exc = 374 nm, em = 420 nm) of **TTPyr3** in DMSO at 298 K, **Figure S15.** Lifetime measurement (exc = 300 nm, em = 470 nm) of **TTPyr3** powders at 298 K, **Figure S16.** Lifetime measurement (exc = 340 nm, em = 520 nm) of **TTPyr3** powders at 298 K, **Figure S17.** Lifetime measurement (exc = 374 nm, em = 394 nm) of **Pyrene** in DMSO at 298 K, **Figure S18.** Photographs of **TTPyr2** (left) and **TTPyr3** (right) solutions under UV light OFF (left) or UV light ON (right, exc = 366 nm), **Figure S19.** Photographs of powders of **TTPyr2** (left) and **TTPyr3** (right) under UV light OFF (left) or UV light ON (right, exc = 366 nm). **Table S1.** Excitation energies (nm), oscillator strength (f) and composition of the first singlet transitions computed for pyrene, **TT-Pyr1** (HT and RT conformations) and **TT-Pyr2** (HT/HT and RT/RT conformations), **Figure S20.** Electronic levels computed for pyrene, **TTPyr1** and **TTPyr2** at molecular level. In blue are reported the singlet levels with oscillator strength f 0.001 and the corresponding values of f (see detailed information in Table S1), **Figure S21.** Simulated absorption spectra of pyrene (top), **TTPyr1**, RT conformation (middle) and **TTPyr2**, RT/RT conformation (bottom) at B97X/6-311++G(d,p) level of theory, resulting from convolution of the singlet excitation energies with 0.1 eV of half-bandwidth (singlet levels plotted as blue sticks according to their oscillator strength), **Figure S22.** Plots of the B97X/6-311++G(d,p) MOs mainly involved in the lowest energy transitions of **TT-Pyr1** in RT conformation (isosurfaces value 0.02), **Figure S23.** Plots of the B97X/6-311++G(d,p) MOs mainly involved in the lowest energy transitions of **TT-Pyr2** in RT/RT conformation (isosurfaces value 0.02). Table S1. Excitation energies, oscillator strength and composition of the first singlet transitions computed for pyrene, **TT-Pyr1** and **TT-Pyr2**.

Author Contributions: Conceptualization, E.C., A.F. and D.M. (Daniele Malpicci); Investigation, D.M. (Daniele Malpicci), D.M. (Daniele Marinotto) and E.L.; Validation, C.G.; Quantum-mechanical calculations, A.F.; Writing the original draft, E.C. and A.F.; Writing—Review and editing, E.C., A.F. and E.L.; Funding acquisition, E.C., A.F. and C.G. All authors have read and agreed to the published version of the manuscript.

Funding: This research received no external funding.

Institutional Review Board Statement: Not applicable.

Informed Consent Statement: Not applicable.

Data Availability Statement: Not applicable.

Acknowledgments: The use of instrumentation purchased through the Regione Lombardia-Fondazione Cariplo joint SmartMatLab Project is gratefully acknowledged.

Conflicts of Interest: The authors declare no conflict of interest.

References

1. Qin, W.; Zhang, P.; Li, H.; Lam, J.W.Y.; Cai, Y.; Kwok, R.T.K.; Qian, J.; Zheng, W.; Tang, B.Z. Ultrabright red AIEgens for two-photon vascular imaging with high resolution and deep penetration. *Chem. Sci.* **2018**, *9*, 2705–2710. [[CrossRef](#)] [[PubMed](#)]
2. Zhi, J.; Zhou, Q.; Shi, H.; An, Z.; Huang, W. Organic Room Temperature Phosphorescence Materials for Biomedical Applications. *Chem. Asian J.* **2020**, *15*, 947–957. [[CrossRef](#)]

3. Gu, L.; Wu, H.; Ma, H.; Ye, W.; Jia, W.; Wang, H.; Chen, H.; Zhang, N.; Wang, D.; Qian, C.; et al. Color-tunable ultralong organic room temperature phosphorescence from a multicomponent copolymer. *Nat. Commun.* **2020**, *11*, 944. [[CrossRef](#)]
4. Lei, Y.; Dai, W.; Guan, J.; Guo, S.; Ren, F.; Zhou, Y.; Shi, J.; Tong, B.; Cai, Z.; Zheng, J.; et al. Wide-Range Color-Tunable Organic Phosphorescence Materials for Printable and Writable Security Inks. *Angew. Chem. Int. Ed.* **2020**, *59*, 16054–16060. [[CrossRef](#)]
5. Hirata, S.; Totani, K.; Kaji, H.; Vacha, M.; Watanabe, T.; Adachi, C. Reversible Thermal Recording Media Using Time-Dependent Persistent Room Temperature Phosphorescence. *Adv. Opt. Mater.* **2013**, *1*, 438–442. [[CrossRef](#)]
6. An, Z.; Zheng, C.; Tao, Y.; Chen, R.; Shi, H.; Chen, T.; Wang, Z.; Li, H.; Deng, R.; Liu, X.; et al. Stabilizing triplet excited states for ultralong organic phosphorescence. *Nat. Mater.* **2015**, *14*, 685–690. [[CrossRef](#)] [[PubMed](#)]
7. Lucenti, E.; Forni, A.; Botta, C.; Carlucci, L.; Giannini, C.; Marinotto, D.; Previtali, A.; Righetto, S.; Cariati, E. H-Aggregates Granting Crystallization-Induced Emissive Behavior and Ultralong Phosphorescence from a Pure Organic Molecule. *J. Phys. Chem. Lett.* **2017**, *8*, 1894–1898. [[CrossRef](#)] [[PubMed](#)]
8. Lucenti, E.; Forni, A.; Botta, C.; Carlucci, L.; Giannini, C.; Marinotto, D.; Pavanello, A.; Previtali, A.; Righetto, S.; Cariati, E. Cyclic Triimidazole Derivatives: Intriguing Examples of Multiple Emissions and Ultralong Phosphorescence at Room Temperature. *Angew. Chem. Int. Ed.* **2017**, *56*, 16302–16307. [[CrossRef](#)] [[PubMed](#)]
9. Ma, X.-K.; Liu, Y. Supramolecular Purely Organic Room-Temperature Phosphorescence. *Acc. Chem. Res.* **2021**, *54*, 3403–3414. [[CrossRef](#)] [[PubMed](#)]
10. Kabe, R.; Adachi, C. Organic long persistent luminescence. *Nature* **2017**, *550*, 384–387. [[CrossRef](#)]
11. Li, D.; Lu, F.; Wang, J.; Hu, W.; Cao, X.-M.; Ma, X.; Tian, H. Amorphous Metal-Free Room-Temperature Phosphorescent Small Molecules with Multicolor Photoluminescence via a Host–Guest and Dual-Emission Strategy. *J. Am. Chem. Soc.* **2018**, *140*, 1916–1923. [[CrossRef](#)]
12. Zhang, Z.; Xu, W.-W.; Xu, W.-S.; Niu, J.; Sun, X.; Liu, Y. A Synergistic Enhancement Strategy for Realizing Ultralong and Efficient Room-Temperature Phosphorescence. *Angew. Chem. Int. Ed.* **2020**, *59*, 18748–18754. [[CrossRef](#)]
13. Hayduk, M.; Riebe, S.; Voskuhl, J. Phosphorescence Through Hindered Motion of Pure Organic Emitters. *Chem. A Eur. J.* **2018**, *24*, 12221–12230. [[CrossRef](#)]
14. Baroncini, M.; Bergamini, G.; Ceroni, P. Rigidification or interaction-induced phosphorescence of organic molecules. *Chem. Commun.* **2017**, *53*, 2081–2093. [[CrossRef](#)]
15. Sun, L.; Zhu, W.; Yang, F.; Li, B.; Ren, X.; Zhang, X.; Hu, W. Molecular cocrystals: Design, charge-transfer and optoelectronic functionality. *Phys. Chem. Chem. Phys.* **2018**, *20*, 6009–6023. [[CrossRef](#)] [[PubMed](#)]
16. Bolton, O.; Lee, K.; Kim, H.-J.; Lin, K.Y.; Kim, J. Activating Efficient Phosphorescence from Purely Organic Materials by Crystal Design. *Nat. Chem.* **2011**, *3*, 205–210. [[CrossRef](#)]
17. Shi, H.; An, Z.; Li, P.-Z.; Yin, J.; Xing, G.; He, T.; Chen, H.; Wang, J.; Sun, H.; Huang, W.; et al. Enhancing Organic Phosphorescence by Manipulating Heavy-Atom Interaction. *Cryst. Growth Des.* **2016**, *16*, 808–813. [[CrossRef](#)]
18. Lin, Z.; Kabe, R.; Nishimura, N.; Jinnai, K.; Adachi, C. Organic Long-Persistent Luminescence from a Flexible and Transparent Doped Polymer. *Adv. Mater.* **2018**, *30*, 1803713. [[CrossRef](#)] [[PubMed](#)]
19. Lucenti, E.; Forni, A.; Botta, C.; Carlucci, L.; Colombo, A.; Giannini, C.; Marinotto, D.; Previtali, A.; Righetto, S.; Cariati, E.M. The Effect of Bromo Substituents on the Multifaceted Emissive and Crystal-Packing Features of Cyclic Triimidazole Derivatives. *ChemPhotoChem* **2018**, *2*, 801–805. [[CrossRef](#)]
20. Lucenti, E.; Forni, A.; Botta, C.; Giannini, C.; Malpicci, D.; Marinotto, D.; Previtali, A.; Righetto, S.; Cariati, E.M. Intrinsic and Extrinsic Heavy-Atom Effects on the Multifaceted Emissive Behavior of Cyclic Triimidazole. *Chem. A Eur. J.* **2019**, *25*, 2452–2456. [[CrossRef](#)] [[PubMed](#)]
21. Giannini, C.; Forni, A.; Malpicci, D.; Lucenti, E.; Marinotto, D.; Previtali, A.; Carlucci, L.; Cariati, E. Room Temperature Phosphorescence from Organic Materials: Unravelling the Emissive Behaviour of Chloro-Substituted Derivatives of Cyclic Triimidazole. *Eur. J. Org. Chem.* **2021**, *2021*, 2041–2049. [[CrossRef](#)]
22. Previtali, A.; Lucenti, E.; Forni, A.; Mauri, L.; Botta, C.; Giannini, C.; Malpicci, D.; Marinotto, D.; Righetto, S.; Cariati, E. Solid State Room Temperature Dual Phosphorescence from 3-(2-Fluoropyridin-4-yl)triimidazo[1,2-a:1',2'-c:1'',2''-e][1,3,5]triazine. *Molecules* **2019**, *24*, 2552. [[CrossRef](#)]
23. Lucenti, E.; Forni, A.; Previtali, A.; Marinotto, D.; Malpicci, D.; Righetto, S.; Giannini, C.; Virgili, T.; Kabacinski, P.; Ganzer, L.; et al. Unravelling the intricate photophysical behavior of 3-(pyridin-2-yl)triimidazotriazine AIE and RTP polymorphs. *Chem. Sci.* **2020**, *11*, 7599–7608. [[CrossRef](#)] [[PubMed](#)]
24. Previtali, A.; He, W.; Forni, A.; Malpicci, D.; Lucenti, E.; Marinotto, D.; Carlucci, L.; Mercandelli, P.; Ortenzi, M.A.; Terraneo, G.; et al. Tunable Linear and Nonlinear Optical Properties from Room Temperature Phosphorescent Cyclic Triimidazole-Pyrene Bio-Probe. *Chem. A Eur. J.* **2021**. [[CrossRef](#)] [[PubMed](#)]
25. Figueira-Duarte, T.M.; Müllen, K. Pyrene-Based Materials for Organic Electronics. *Chem. Rev.* **2011**, *111*, 7260–7314. [[CrossRef](#)]
26. De Silva, T.P.D.; Youm, S.G.; Fronczek, F.R.; Sahasrabudhe, G.; Nesterov, E.E.; Warner, I.M. Pyrene-Benzimidazole Derivatives as Novel Blue Emitters for OLEDs. *Molecules* **2021**, *26*, 6523. [[CrossRef](#)] [[PubMed](#)]
27. Yang, J.; Qin, J.; Ren, Z.; Peng, Q.; Xie, G.; Li, Z. Pyrene-Based Blue AIEgen: Enhanced Hole Mobility and Good EL Performance in Solution-Processed OLEDs. *Molecules* **2017**, *22*, 2144. [[CrossRef](#)]
28. Schubert, D.M.; Natan, D.T.; Wilson, D.C.; Hardcastle, K.I. Facile Synthesis and Structures of Cyclic Triimidazole and Its Boric Acid Adduct. *Cryst. Growth Des.* **2011**, *11*, 843–850. [[CrossRef](#)]

29. Suzuki, K.; Kobayashi, A.; Kaneko, S.; Takehira, K.; Yoshihara, T.; Ishida, H.; Shiina, Y.; Oishi, S.; Tobita, S. Reevaluation of absolute luminescence quantum yields of standard solutions using a spectrometer with an integrating sphere and a back-thinned CCD detector. *Phys. Chem. Chem. Phys.* **2009**, *11*, 9850–9860. [[CrossRef](#)]
30. Chai, J.-D.; Head-Gordon, M. Systematic optimization of long-range corrected hybrid density functionals. *J. Chem. Phys.* **2008**, *128*, 084106. [[CrossRef](#)]
31. Frisch, M.J.; Trucks, G.W.; Schlegel, H.B.; Scuseria, G.E.; Robb, M.A.; Cheeseman, J.R.; Scalmani, G.; Barone, V.; Petersson, G.A.; Nakatsuji, H.; et al. *Gaussian 16*; Revision. A. 03; Gaussian Inc.: Wallingford, CT, USA, 2016.
32. Bader, R.F.W. *Atoms in Molecules: A Quantum Theory*; Clarendon Press: Oxford, UK, 1990.
33. Bader, R.F.W. Bond Paths Are Not Chemical Bonds. *J. Phys. Chem. A* **2009**, *113*, 10391–10396. [[CrossRef](#)]
34. Pendás, A.M.; Francisco, E.; Blanco, M.A.; Gatti, C. Bond Paths as Privileged Exchange Channels. *Chem. A Eur. J.* **2007**, *13*, 9362–9371. [[CrossRef](#)] [[PubMed](#)]
35. Winnik, F.M. Photophysics of preassociated pyrenes in aqueous polymer solutions and in other organized media. *Chem. Rev.* **1993**, *93*, 587–614. [[CrossRef](#)]
36. Lee, S.H.; Kim, S.H.; Kim, S.K.; Jung, J.H.; Kim, J.S. Fluorescence Ratiometry of Monomer/Excimer Emissions in a Space-Through PET System. *J. Org. Chem.* **2005**, *70*, 9288–9295. [[CrossRef](#)] [[PubMed](#)]
37. Suzuki, I.; Ui, A.M.; Yamauchi, A. Supramolecular Probe for Bicarbonate Exhibiting Anomalous Pyrene Fluorescence in Aqueous Media. *J. Am. Chem. Soc.* **2006**, *128*, 4498–4499. [[CrossRef](#)]
38. Wrona-Piotrowicz, A.; Makal, A.; Zakrzewski, J. Triflic Acid-Promoted Adamantylation and tert-Butylation of Pyrene: Fluorescent Properties of Pyrene-Decorated Adamantanes and a Channeled Crystal Structure of 1,3,5-Tris(pyren-2-yl)adamantane. *J. Org. Chem.* **2020**, *85*, 11134–11139. [[CrossRef](#)] [[PubMed](#)]
39. Kotchapradist, P.; Prachumrak, N.; Tarsang, R.; Jungsuttiwong, S.; Keawin, T.; Sudyoasuk, T.; Promarak, V. Pyrene-functionalized carbazole derivatives as non-doped blue emitters for highly efficient blue organic light-emitting diodes. *J. Mater. Chem. C* **2013**, *1*, 4916–4924. [[CrossRef](#)]